Journal of Solid State Chemistry 184 (2011) 214–219

Contents lists available at ScienceDirect

Journal of Solid State Chemistry

journal homepage: www.elsevier.com/locate/jssc

A new series of lanthanoid containing Keggin-type germanotungstates with acetate chelators: $[\{Ln(CH_3COO)GeW_{11}O_{39}(H_2O)\}_2]^{12-}$ {Ln=Eu^{III}, Gd^{III}, Tb^{III}, Dy^{III}, Ho^{III}, Er^{III}, Tm^{III}, and Yb^{III}}

Firasat Hussain [a,*,1], Stefan Sandriesser [a], Manfred Speldrich [b], Greta R. Patzke [a,*]

[a] Institute of Inorganic Chemistry, University of Zurich, Winterthurerstrasse 190, CH-8057 Zurich, Switzerland
[b] Institute of Inorganic Chemistry, RWTH Aachen University, D-52074 Aachen, Germany

ARTICLE INFO

Article history:
Received 30 April 2010
Received in revised form
19 October 2010
Accepted 8 November 2010
Available online 13 November 2010

Keywords:
Polyoxotungstates
Germanium
Gadolinium
Magnetism
Lanthanoids

ABSTRACT

A series of head-on complexes of lanthanoid containing germanotungstates was isolated from a one pot reaction in an acetate buffer at pH 4.5. This convenient approach brought forward the $[\{Ln(CH_3COO)GeW_{11}O_{39}(H_2O)\}_2]^{12-}$ (Ln=Eu^{III}, Gd^{III}, Tb^{III}, Dy^{III}, Ho^{III}, Er^{III}, Tm^{III}, and Yb^{III}) family with acetate chelators in the rarely observed μ_2: η^2–η^1 mode. All compounds were structurally characterized using various solid state analytics, such as single crystal X-ray diffraction, FT-IR spectroscopy, and thermogravimetric analysis. The isostructural polyanions crystallize in the monoclinic system (S.G. $P2_1/c$). Temperature-dependent magnetic susceptibility measurements were performed on the Gd^{III}-complex which exhibits near perfect Curie-type behavior.

1. Introduction

Polyoxometalates (POMs) are metal oxide nanoclusters with metals in their high oxidation states that keep attracting worldwide research interest due to their almost endless variety of molecular architectures [1–9]. POMs are usually obtained from aqueous media and their impressive range of potential applications is another driving force for investigating their synthetic pathways. Furthermore, their use in medicine [10], catalysis [11,12], multifunctional materials, imaging, bio- and nanotechnology is just about to be fully explored [13,14].

Among the continuously growing family of POMs, their lanthanoid-containing representatives are of special interest due to their magnetic and luminescent properties [15–24]. In addition, they are promising candidates for the development of Lewis-acid catalysts, and Gd-POMs in particular are used for new magnetic resonance imaging (MRI) contrast agents [25]. In the course of our previous studies, we have explored the formation of *Ln*-POMs from lanthanoid cations and lacunary POMs with respect to the development of synthetic strategies for large clusters: firstly, the oxophilic cations match well with the lacunary POMs to generate high nuclear polyoxoanions with unprecedented shape and size. Secondly, the lanthanoid cations are exceptionally versatile structural linkers due to their high coordination numbers [26].

This is impressively illustrated by the largest polyoxotungstate known to date, namely the cerium-containing polyoxotungstoarsenate(III) $[Ce_{16}As_{12}(H_2O)_{36}W_{148}O_{524}]^{76-}$ that was reported by Pope in 1997 [27]. The second-largest representative was another Ce-POM, $[Ce_{20}Ge_{10}W_{100}O_{376}(OH)_4(H_2O)_{30}]^{56-}$, that was discovered a decade later by Kortz et al. [28]. Recently, we have demonstrated that the formation of large discrete polyoxotungstates is not only limited to the early lanthanoid ions, but can also be extended upon the mid and late members of the series as has been shown by the formation of the $[Gd_8As_{12}W_{124}O_{432}(H_2O)_{22}]^{60-}$ and $[Yb_{10}As_{10}W_{88}O_{308}(OH)_8(H_2O)_{28}(OAc)_4]^{40-}$ polyanions and by our recently published $[Ln_{16}As_{16}W_{164}O_{576}(OH)_8(H_2O)_{42}]^{80-}$ (Ln=Eu^{III}, Gd^{III}, Tb^{III}, Dy^{III}, Ho^{III}) polyanions [26c, a, d].

Although such hybrid clusters are in the focus of many other groups (e.g. Müller, Francesconi, Yamase, Krebs, Kortz, Gouzerh, Sécheresse, Hill, Wang) [15–24], our current studies on *Ln*-POMs indicate that there is still plenty of room to discover novel molecular architectures that can be tailored for current applications, e.g. in materials research and biochemistry.

In the following, we present the syntheses and structural characterization of a series of mid- and late lanthanoid containing POMs of the $Na_4K_8[\{Ln(CH_3COO)GeW_{11}O_{39}(H_2O)\}_2]\cdot xH_2O$ type (Ln=Eu^{III} (**1**), Gd^{III} (**2**), Tb^{III} (**3**), Dy^{III} (**4**), Ho^{III} (**5**), Er^{III} (**6**), Tm^{III} (**7**), and Yb^{III} (**8**)); (**NaK-{*Ln*-GeW$_{11}$}**).

* Corresponding authors. Fax: +41 44 635 6802.
E-mail address: greta.patzke@aci.uzh.ch (G.R. Patzke).
[1] Present address: Department of Chemistry, Nanoscience and Nanotechnology, University of Delhi, 110 007, India.

0022-4596/$ - see front matter © 2010 Elsevier Inc. All rights reserved.
doi:10.1016/j.jssc.2010.11.005

2. Experimental section

2.1. General procedures

$Na_{10}(\alpha\text{-}GeW_9O_{34})$ was synthesized as reported by Hervé and Tézé [29]. All lanthanoid sources were purchased from Sigma-Aldrich and used without further purification.

Fourier transform infrared (FT-IR) spectra were recorded on a Perkin-Elmer BXII spectrometer with KBr pellets. TG measurements were performed on a Netzsch STA 449C between 25 and 600 °C with a heating rate of 5 °C/min in nitrogen atmosphere. Magnetic susceptibility measurements were performed on a Quantum Design DC-SQUID magnetometer (5.5 TMPMS). Elemental analyses were performed by Mikroanalytisches Labor Pascher, Remagen, Germany.

2.2. Synthesis of the NaK-{Ln-GeW_{11}} series

$Na_4K_8[\{Eu(CH_3COO)GeW_{11}O_{39}(H_2O)\}_2]\cdot 20H_2O$–(Eu-1): A sample of A-$Na_{10}(\alpha\text{-}GeW_9O_{34})$ (0.526 g (0.15 mmol)), was added under stirring to a solution of 0.193 g (0.45 mmol) $Eu(NO_3)_3\cdot 6H_2O$ in 25 mL 1 M CH_3COOH–CH_3COOK buffer at pH 4.7. The solution was heated to 50 °C for 30 min and then filtered. The colorless filtrate was subjected to slow evaporation at room temperature which afforded a colorless crystalline product (diamond-plate shaped crystals) after ca. four weeks. Yield: 0.314 g (43%). FTIR: 1625(s), 1534(m), 1451(m), 1398(m), 950(s), 896(s), 810(w), 749(sh), 678(w), 533(m), 470(m) (cm^{-1}). Elemental analysis (%); calcd. (found): Na 1.0 (0.6), K 5.2 (5.6), W 59.8 (59.2), Ge 2.1 (2.1), Eu 4.5 (4.4). This experimental protocol provides the following complexes (**Gd-2**–**Yb-8**) in comparable yields.

$Na_4K_8[\{Gd(CH_3COO)GeW_{11}O_{39}(H_2O)\}_2]\cdot 20H_2O$–(Gd-2): Experimental procedure cf. above, 0.203 g (0.45 mmol) $Gd(NO_3)_3\cdot 6H_2O$ was used instead of $Eu(NO_3)_3\cdot 6H_2O$. FTIR: 1625(s), 1532(m), 1450(m), 1401(m), 950(s), 882(s), 810(w), 746(sh), 676(w), 529(m), 468(m), 449(w), (cm^{-1}). Elemental analysis (%); calcd. (found): Na 1.0 (0.6), K 5.2 (5.3), W 59.7 (59.3), Ge 2.1 (2.2), Gd 4.6 (4.6).

$Na_4K_8[\{Tb(CH_3COO)GeW_{11}O_{39}(H_2O)\}_2]\cdot 18H_2O$–(Tb-3): Experimental procedure cf. above, $Tb(NO_3)_3\cdot 6H2O$ (0.196 g, 0.45 mmol) was used instead of $Gd(NO_3)_3\cdot 6H_2O$. FTIR: 1626(s), 1532(m), 1455(m), 1399(m), 954(s), 889(s), 810(w), 750(sh), 681(w), 525(m), 470(m), 449(w) (cm^{-1}).

$Na_4K_8[\{Dy(CH_3COO)GeW_{11}O_{39}(H_2O)\}_2]\cdot 16H_2O$–(Dy-4): Experimental procedure cf. above, $Dy(NO_3)_3\cdot 6H_2O$ (0.198 g, 0.45 mmol) was used instead of $Gd(NO_3)_3\cdot 6H_2O$. FTIR: 1626(s), 1536(m), 1455(m), 1401(m), 954(s), 887(s), 813(w), 749(sh), 681(w), 526(m), 468(m), 449(w) (cm^{-1}).

$Na_4K_8[\{Ho(CH_3COO)GeW_{11}O_{39}(H_2O)\}_2]\cdot 18H_2O$–(Ho-5): Experimental procedure cf. above, $Ho(NO_3)_3\cdot 6H_2O$ (0.199 g, 0.45 mmol) was used instead of $Gd(NO_3)_3\cdot 6H_2O$. FTIR: 1627(s), 1538(m), 1456(m), 1405(m), 953(s), 886(s), 814(w), 750(sh), 683(w), 526(m), 469(m), 449(w) (cm^{-1}).

$Na_4K_8[\{Er(CH_3COO)GeW_{11}O_{39}(H_2O)\}_2]\cdot 18H_2O$–(Er-6): Experimental procedure cf. above, $Er(NO_3)_3\cdot 6H_2O$ (0.199 g, 0.45 mmol) was used instead of $Gd(NO_3)_3\cdot 6H_2O$. FTIR: 1624(s), 1540(m), 1459(m), 1384(m), 958(s), 889(s), 813(w), 751(sh), 680(w), 525(m), 466(m), 449(w) (cm^{-1}).

$Na_{4.4}K_{7.6}[\{Tm(CH_3COO)GeW_{11}O_{39}(H_2O)\}_2]\cdot 16H_2O$–(Tm-7): Experimental procedure cf. above, $Yb(NO_3)_3\cdot 6H_2O$ (0.200 g, 0.45 mmol) was used instead of $Gd(NO_3)_3\cdot 6H_2O$. FTIR: 1624(s), 1540(m), 1459(m), 958(s), 889(s), 813(w), 751(sh), 680(w), 525(m), 466(m), 449(w) (cm^{-1}).

$Na_4K_8[\{Yb(CH_3COO)GeW_{11}O_{39}(H_2O)\}_2]\cdot 18H_2O$–(Yb-8): Experimental procedure cf. above, $Tm(NO_3)_3\cdot 6H_2O$ (0.200 g, 0.45 mmol) was used instead of $Gd(NO_3)_3\cdot 6H_2O$. FTIR: 1626(s), 1563(m), 1461(m), 1384(s) 957(s), 890(s), 818(w), 756(sh), 680(w), 525(m), 466(m), 449(w) (cm^{-1}).

2.3. X-ray crystallography

Single crystal X-ray data for compounds **Eu-1**, **Gd-2**, **Tb-3**, **Ho-5**, **Er-6**, **Tm-7**, and **Yb-8** were collected on an Oxford Xcalibur Ruby CCD single-crystal diffractometer (Mo$K\alpha$ radiation, $\lambda = 0.71073$ Å). Routine Lorentz and polarization corrections were applied, and an absorption correction was performed using the ABSCALE 3 program [30]. Direct methods were used to locate the heavy metal atoms (SHELXS-97). The remaining atoms were located from successive Fourier maps (SHELXL-97) [31]. No suitable crystals of **Dy-4** could be obtained for structure determination due to difficulties in crystal growth. A summary of the crystallographic data and structure refinement for all compounds is given in Table 1. Further details on the crystal structure data can be obtained from the Cambridge Crystallographic Data Center via www.ccdc.chem.ac.uk/data_request/cif, on quoting the depository numbers CCDC-767762–767768 for compounds **Eu-1** to **Yb-8**.

Table 1
Crystallographic data and structure determination of **Eu-1**, **Gd-2**, **Tb-3**, **Ho-5**, **Er-6**, **Tm-7**, and **Yb-8**.

Polyanion	Eu-1	Gd-2	Tb-3	Ho-5	Er-6	Tm-7	Yb-8
Empirical formula	$C_4H_6Eu_2Ge_2K_8Na_4O_{111}W_{22}$	$C_4H_6Gd_2Ge_2K_8Na_4O_{110}W_{22}$	$C_4H_6Ge_2K_8Na_4O_{110}Tb_2W_{22}$	$C_4H_6Ge_2HO_2K_{760}Na_4O_{110}W_{22}$	$C_4H_6Er_2Ge_2K_8Na_4O_{110}W_{22}$	$C_4H_6Ge_2K_{7.6}Na_{4.4}O_{108}Tm_2W_{22}$	$C_4H_6Ge_2K_8Na_2O_{108}W_{22}Yb_2$
M_r	6728.65	6723.23	6726.57	6722.95	6743.25	6702.10	6676.83
Space group	$P2_1/c$	$P2_1/c$	$P2_1/c$	$P2_1/c$	$P2_1/c$	$P2_1/c$	$P2_1/c$
a (Å)	20.085(3)	20.1264(2)	20.1171(5)	20.1294(7)	20.1187(6)	20.0982(9)	19.9221(2)
b (Å)	12.6741(9)	12.6758(10)	12.6768(2)	12.6712(3)	12.6618(2)	12.6573(3)	12.56720(10)
c (Å)	21.132(2)	21.1523(2)	21.1300(5)	21.1602(6)	21.1639(5)	21.1193(7)	20.9741(2)
β (°)	110.983(15)	110.839 (10)	110.886(3)	111.011(4)	110.858(3)	110.987(4)	111.2630(10)
V (Å^3)	5022.7(10)	5043.33(8)	5034.51(19)	5038.3(3)	5038.0(2)	5016.1(3)	4893.71(8)
T (K)	183(2)	183(2)	183(2)	183(2)	183(2)	183(2)	183(2)
λ (Å)	0.71073	0.71073	0.71073	0.71073	0.71073	0.71073	0.71073
$d_{calcd.}$(Mg m^{-3})	4.449	4.442	4.437	4.432	4.445	4.476	4.531
μ (mm^{-1})	27.367	27.338	27.460	27.590	27.704	27.927	28.704
Z	2	2	2	2	2	2	2
GooF (on F^2)	0.789	0.976	0.942	0.895	0.804	0.796	1.032
R_1[a] [I > 2σ(I)][a]	0.0484	0.0346	0.0461	0.0537	0.0386	0.0403	0.0453
wR_2[b] (all data)[b]	0.0665	0.0736	0.0882	0.1041	0.0592	0.0596	0.1271

[a] $R = \Sigma\mathrm{II}F_o\mathrm{I}-\mathrm{I}F_c\mathrm{II}/\Sigma\mathrm{I}F_o\mathrm{I}$.
[b] $R_w = [\Sigma w(F_o^2-F_c^2)^2/\Sigma w(F_o^2)^2]^{1/2}$.

3. Results and discussion

3.1. Synthesis

All compounds of the new polyoxotungstate family were synthesized from one pot reactions of the trilacunary POM A-(α-GeW_9O_{34}) with Ln^{III} cations in 1 M CH_3COOH–CH_3COOK buffer. In this way, we conveniently accessed the entire compound series with a common synthetic protocol. Single crystal X-ray diffraction investigations revealed that all compounds of the isostructural title series consist of two {α-$GeW_{11}O_{39}$} units, two lanthanoid cations and two chelating acetate moieties, respectively. Each acetate chelator is connected to the lanthanoid cations in μ_2: η^2–η^1 mode.

In the course of the reaction, the trilacunary POM precursor A-(α-GeW_9O_{34}) incorporates two additional tungsten octahedra to form the monolacunary A-(α-$GeW_{11}O_{39}$) unit. This fragment later reacts with the oxophilic lanthanoid acetate chelator to form the monomer (see Fig. 1). The title anion is subsequently formed through dimerization of the monomeric moiety in the solid state.

3.2. Crystal structures

All compounds of the $[\{Ln(CH_3COO)GeW_{11}O_{39}(H_2O)\}_2]^{12-}$ type were isolated as mixed sodium/potassium salts with a monoclinic crystal structure (S.G. $P2_1/c$). They can be described as organic–inorganic hybrid compounds consisting of two mono-substituted $\{Ln(CH_3COO)GeW_{11}O_{39}(H_2O)\}^{6-}$ fragments (see Fig. 2).

As mentioned above, each of these fragments is bridged by two actetate chelators in the μ_2: η^2–η^1 mode that has first been observed by Kortz et al. [32] for the $[\{La(CH_3COO)(H_2O)(\alpha_2\text{-}P_2W_{17}O_{61})\}_2]^{16-}$ polyanion. Mialane et al. [22] first brought

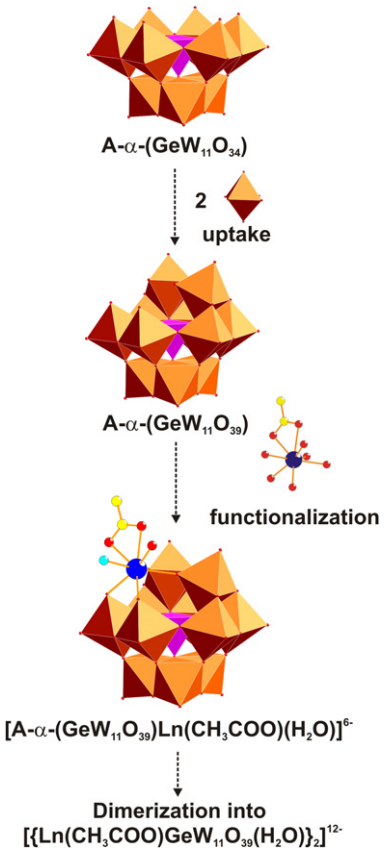

Fig. 1. Schematic representation of the formation of the monomeric $[A\text{-}\alpha\text{-}(GeW_{11}O_{39})Ln(CH_3COO)(H_2O)]^{6-}$ moiety.

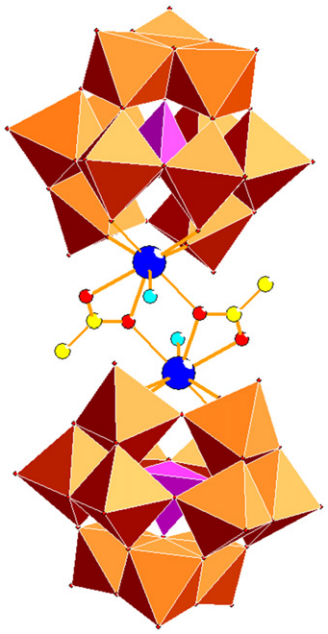

Fig. 2. Polyhedron representation of $[\{Ln(CH_3COO)GeW_{11}O_{39}(H_2O)\}_2]^{12-}$ (Ln=Eu^{III}, Gd^{III}, Tb^{III}, Ho^{III}, Er^{III}, Tm^{III}, and Yb^{III}; W: orange; Ge: pink; *Ln*: blue; O: red; C: yellow; H_2O: cyan). (For interpretation of the references to color in this figure legend, the reader is referred to the web version of this article.)

forward the $[\{Ln(CH_3COO)SiW_{11}O_{39}(H_2O)\}_2]^{12-}$ (Ln=Gd^{III} and Yb^{III}) type starting from the according $K_5[Ln(SiW_{11}O_{39})(H_2O)_2]\cdot 24H_2O$ precursors.

This bridging type furthermore occurs in the Gd-containing compound $[Gd_6As_6W_{65}O_{229}(OH)_4(H_2O)_{12}(OAc)_2]^{38-}$ that was recently reported by one of us [26a]. It is to be noted that this connection mode is still rarely observed in POM chemistry. Therefore, we have developed a new strategy in the present study: whilst $[\{Ln(CH_3COO)SiW_{11}O_{39}(H_2O)\}_2]^{12-}$ (Ln=Gd^{III} and Yb^{III}) [22] were synthesized by dissolution of $K_5[\{LnSiW_{11}O_{39}(H_2O)_2\}]\cdot 24H_2O$ in 2 M acetate buffer, we developed a one-step approach starting from the interaction of the A-type Na_{10}(α-GeW_9O_{34}) ligand with Ln^{III} cations in 1 M CH_3COOH–CH_3COOK buffer solution.

Recently, Wang et al. reported on a series of lanthanoid containing phosphotungstate complexes, which were synthesized through a one pot reaction in sodium acetate buffer. In order to obtain crystals of good quality, however, the alkali cations had to be ion exchanged by organic cations in a follow-up step [24].

The crystal packing motif of the isostructural polyanion series is constituted of isolated $[\{Ln(CH_3COO)GeW_{11}O_{39}(H_2O)\}_2]^{12-}$ complexes that are electrostatically connected via alkali cations into a layered motif. The Ln^{III} cations are "sandwiched" between the layers along the *b* and *c* axes in a ladder-like arrangement that is especially pronounced in the *c* direction (Fig. 3).

Both lanthanoid centers of the dimeric title compound display a square-antiprismatic eightfold coordination (pseudo-D_{4d}, cf. Fig. 4) with three oxygen atoms contributed from the acetate chelator, four oxygen atoms from the monovacant A-(α-$GeW_{11}O_{39}$) unit and the last one from the attached terminal water molecule (representative bond distances are provided in Table 2 for **Gd-2**). The average distance between the *Ln* and O atoms is in the range 2.35–2.41 Å. These interatomic distances are particularly sensitive to the lanthanide contraction so that they decrease with the radius of the trivalent *Ln* ion (Fig. 5) [33]. One oxygen atom of the eightfold *Ln* coordination sphere is exclusively coordinated to the *Ln* atom and the corresponding *Ln*–O distance range of 2.42–2.33 Å clearly illustrates the influence of the *Ln* radii on the local environments. Furthermore, the *Ln*–*Ln* bond distances decrease

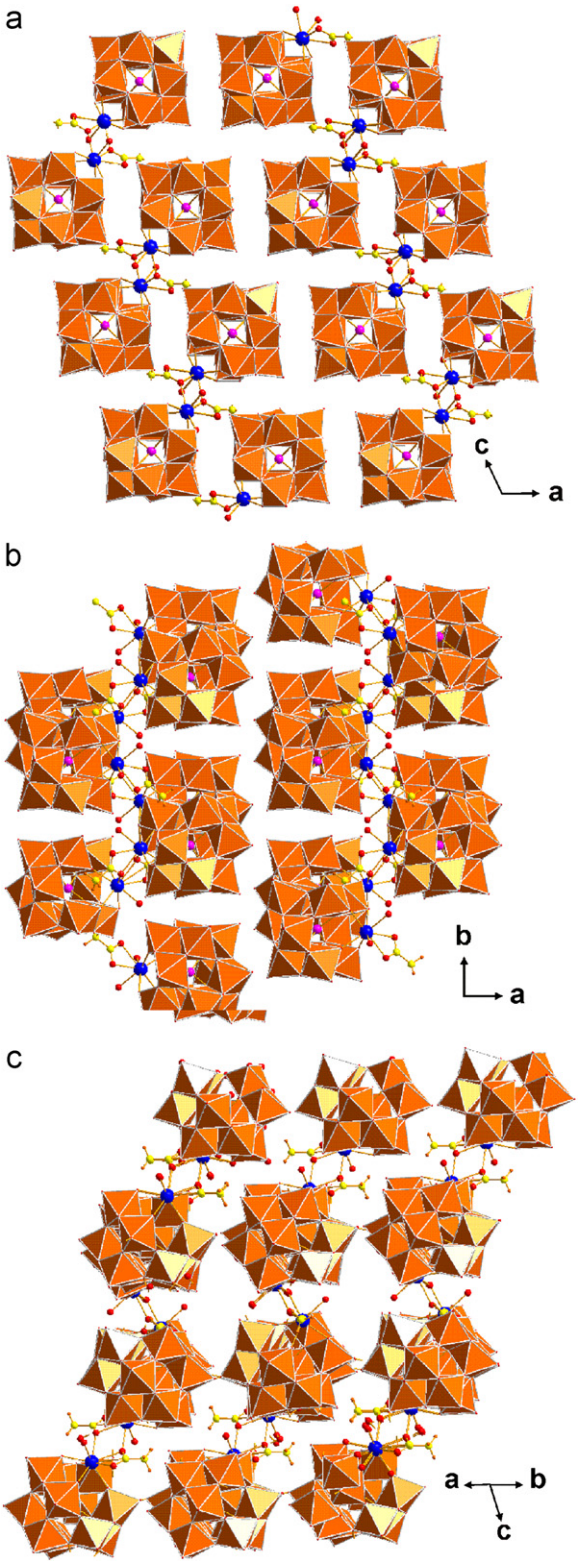

Fig. 3. Packing arrangement of the polyanions $[\{Ln(CH_3COO)GeW_{11}O_{39}(H_2O)\}_2]^{12-}$ (Ln=Eu^{III}, Gd^{III}, Tb^{III}, Ho^{III}, Er^{III}, Tm^{III}, and Yb^{III}) along different directions (W: orange polyhedra; Ge: pink; *Ln*: blue; O: red; C: yellow; cations and crystal water are omitted for clarity). (For interpretation of the references to color in this figure legend, the reader is referred to the web version of this article.)

from 4.19 to 4.11 Å, and this trend also reflects the lanthanoid contraction (Fig. 5) [34]. A tentative overall decrease of the lattice constant with the *Ln* radius can be observed for the *b* axis (Fig. 5),

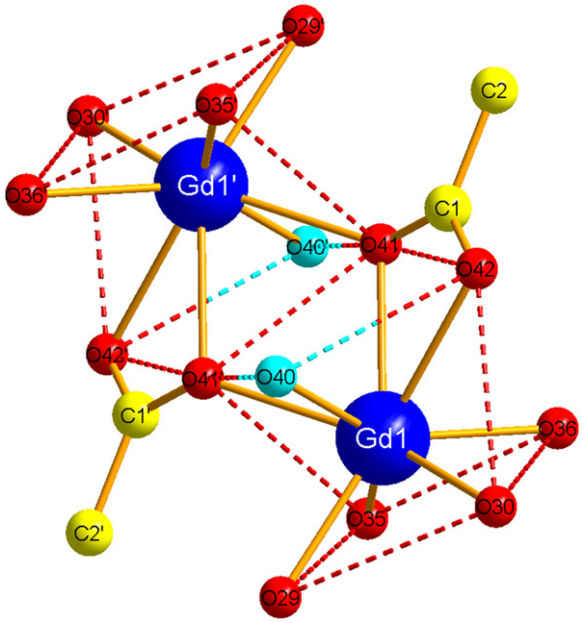

Fig. 4. Square-antiprismatic coordination environment of the lanthanoid ions (indicated with dotted lines; Gd: blue; O: red; C: yellow). (For interpretation of the references to color in this figure legend, the reader is referred to the web version of this article.)

Table 2
Selected bond lengths (Å) of polyanion **Gd-2**.

Atoms	Bond length (Å)
C(1)–O(41)	1.29(1)
C(1)–O(42)	1.24(2)
C(1)–C(2)	1.508(1)
O(29)–W(4)	1.766(6)
O(30)–W(5)	1.797(6)
O(36)–W(10)	1.786(5)
O(35)–W(11)	1.765(6)
O(29)–Gd(1)	2.357(7)
O(30)–Gd(1)	2.371(6)
O(36)–Gd(1)	2.344(6)
O(35)–Gd(1)	2.318(7)
O(40)–Gd(1)	2.410(1)
O(41)–Gd(1)	2.504(6)
O(42)–Gd(1)	2.518(8)

whereas the other directions display a less regular trend and thus probably weaker *Ln* connectivity in these directions. The resulting cell volume as a function of the *Ln* radius is more or less an overlay of the individual lattice constant curves (Fig. 5). The decrease in cell volumes is only significant for the last three cations in the series (Er–Yb): this indicates that the effect of the lanthanoid contraction on the structural parameters is obviously more significant for the local polyoxometalate geometry than for the overall crystal packing.

According to bond valence sum (BVS) calculations [35], none of the oxygen atoms of the two (α-$GeW_{11}O_{39}$) units in the dimeric entity is protonated and two terminal dihydroxo ligands were located on the lanthanoid atoms. As none of the *Ln*–O–W (*Ln*=Eu^{III}, Gd^{III}, Tb^{III}, Dy^{III}, Ho^{III}, Er^{III}, Tm^{III}, and Yb^{III}) bridges are mono- or diprotonated, the net charge of the title polyanion $[\{Ln(CH_3COO)GeW_{11}O_{39}(H_2O)\}_2]^{12-}$ can be assigned as −12 and it is balanced by sodium and potassium countercations in the solid state.

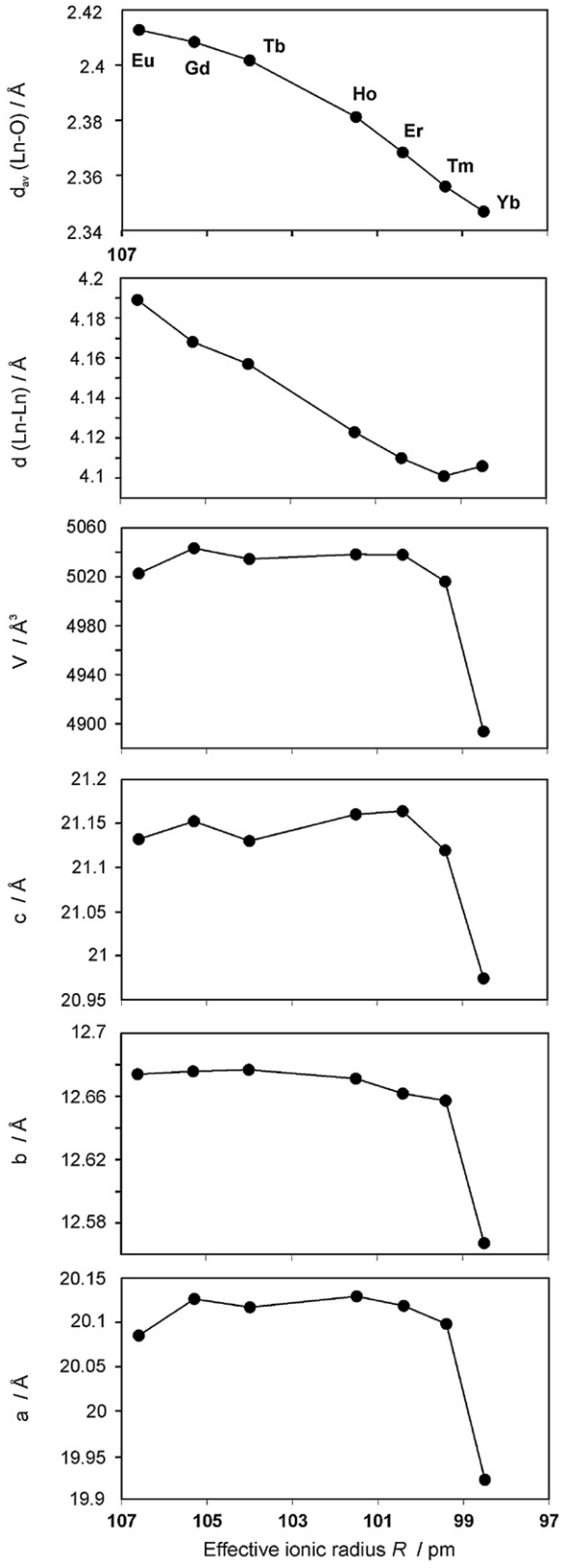

Fig. 5. Variations in the bond distances and lattice parameters plotted against the effective ionic radii of eight-coordinated Ln^{3+} ions.

3.3. IR spectroscopy and thermogravimetric analysis

The FT-IR spectra of polyanions **NaK-{*Ln*-GeW$_{11}$}** (Ln=Eu^{III}, Gd^{III}, Tb^{III}, Dy^{III}, Ho^{III}, Er^{III}, Tm^{III}, and Yb^{III}) display closely related characteristic stretching frequencies in the 2000–400 cm^{-1} region (cf. 2.2.) and their comparison clearly shows that all compounds are isostructural (cf. Fig. SI-1). In particular, the bands in the range from 1000 to 400 cm^{-1} represent the "*fingerprint region*" of the polyoxometalate ligand. For the title polyanions **NaK-{*Ln*-GeW$_{11}$}** frequencies at 477 or 467 cm^{-1} correspond to δ(O–Ge–O), whereas bands at 890–896 cm^{-1} correspond to ν_{as}(W–O$_b$–W). The frequencies in the 745–750 cm^{-1} range represent ν_{as}(W–O$_c$–W) and bands at 950–958 cm^{-1} stand for ν_{as}(W=O$_d$). Furthermore, four distinct stretching frequencies observed in the region from 1400 to 1627 cm^{-1} correspond to the ν_{as}(C=O) and ν_{as}(C–O) of the acetate ligands bridged to the metal center in μ_2: η^2–η^1 mode [24,36].

Thermogravimetric analysis were performed on the solid samples of polyanions **NaK-{*Ln*-GeW$_{11}$}** in the temperature range between 25 and 600 °C to quantify the amount of crystal water molecules present in the compounds. The mass loss corresponds to 16–20 water molecules along the series (cf. Section 2.2 and Fig. SI-2).

3.4. Magnetic measurements

Gd-2 was selected for magnetic measurements in order to model all relevant single-ion parameters for the most clearly arranged magnetic system among the series. Preliminary variable-temperature magnetic susceptibility data for compound **Gd-2** (5–250 K, 0.2 T) reveal spin-only magnetism under consideration of the applied field (B_0) for the Gd(III) ($L\approx 0$, $S=7/2$)-based species with a near perfect Curie-type temperature dependence of the molar magnetic susceptibility ($C=9.836\times10^{-5}$ m^3 kmol^{-1}). The corresponding effective magnetic moment is equal to 7.91 μ_B. The program CONDON has proven especially suitable to analyze the magnetic susceptibility of transition metal and lanthanoid systems [37]. Simulations of the magnetic behavior using CONDON consider interelectronic repulsion (H_{ee}), spin-orbit coupling (H_{so}), a ligand-field effect (H_{lf}) and the applied field (H_{mag}) [38]. Compound **Gd-2** with two Gd(III) centers ($4f^7$, $^8S_{7/2}$) approaches a room-temperature effective magnetic moment of 7.91 μB (cf. Fig. 6) which is in good agreement with the corresponding spin-only value for a single Gd(III) ion of 7.91 μ_B with a g value of 1.993 [38]. The slightly reduced g-value is a result of the large spin–orbit interaction that mixes significant amounts of other terms with $J=7/2$ into the ground state [38]. The major *SL* components of the ground state are ^8S (97%) and ^6P (2.7%) with the corresponding g_J factor 1.993 [39]. This suggests predominantly

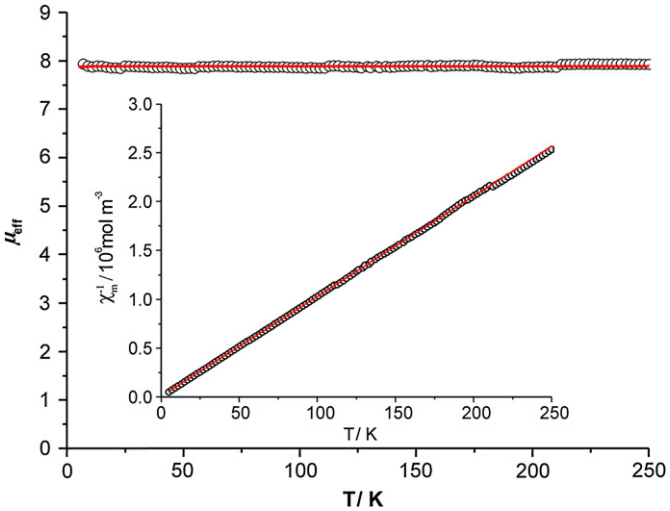

Fig. 6. Effective magnetic moment vs. T plot of **Gd-2** per one Gd(III)-ion in the temperature range 5–250 K at an applied field of B_0=0.2 T (exp. data: open circles; best fits: solid lines; parameter values cf. text).

uncoupled behavior of the individual gadolinium centers, and no exchange interactions are observed.

The following Slater–Condon parameters were taken into account to determine the magnetic behavior of **Gd-2**: $^2F=91800\ cm^{-1}$, $^4F=64425\ cm^{-1}$, $^6F=49258\ cm^{-1}$, the spin–orbit-coupling constant ($\zeta=1470\ cm^{-1}$) and the applied magnetic field ($B_0=0.2$ T) [40].

4. Conclusions

In conclusion, we have isolated a series of lanthanoid-containing germanotungstates that were obtained from a one pot strategy in 1 M CH_3COOH–CH_3COOK buffer solutions. The synthetic protocol provides a facile access to single crystalline organic-inorganic composites containing actetate chelators in the less commonly observed μ_2: η^2–η^1 mode. Moreover, these head-on actetate bridged POM dimers have been structurally characterized for the first time for germanotungstates. The lanthanoid contraction among the novel compound series is reflected in a general decrease of the *Ln*–*Ln* distances, and the average *Ln*–O distances of the square-antiprismatic lanthanoid coordination environments follow the same trend. The Curie-type magnetic susceptibility of the Gd-representative corresponds with the observed distance between the lanthanoid centers and the experimental results are well in line with simulations of the magnetic behavior. This new subtype of the family of lanthanoid-containing polyoxometalates once more demonstrates the inexhaustible potential of lanthanoid-assisted approaches for the construction of POM architectures. The compound series is furthermore an interesting starting point for more detailed magnetic measurements and for studies of their photo-physical and bio-medical properties.

Acknowledgments

This work was supported by the Swiss National Science Foundation (SNSF Professorship PP002-114711/1) and financial support from the University of Zurich is gratefully acknowledged.

Appendix A. Supplementary material

Supplementary data associated with this article can be found in the online version at doi:10.1016/j.jssc.2010.11.005.

References

[1] M.T. Pope, Heteropoly and Isopoly Oxometalates, Springer, Berlin, 1983.
[2] M.T. Pope, A. Müller, Angew. Chem. 103 (1991) 56–70;
M.T. Pope, A. Müller, Angew. Chem. Int. Ed. 30 (1991) 34–48.
[3] M.T. Pope, Compr. Coord. Chem. II 4 (2003) 635–678.
[4] C.L. Hill, Compr. Coord. Chem. II 4 (2003) 679–759;
C.L. Hill, C.M. Prosser-McCartha, Coord. Chem. Rev. 143 (1995) 407–455.
[5] L. Cronin, Compr. Coord. Chem. II. 7 (2003) 1–56.
[6] J.J. Borras-Almenar, E. Coronado, A. Müller, M.T. Pope (Eds.), Polyoxometalate Molecular Science, Kluwer, Dordrecht, 2004.
[7] M.T. Pope, A. Müller (Eds.), Polyoxometalates: from Platonic Solids to Anti-retroviral Activity, Kluwer, Dordrecht, 1994.
[8] U. Kortz, A. Müller, J. van Slageren, J. Schnack, N.S. Dalal, M. Dressel, Coord. Chem. Rev. 253 (2009) 19–20.
[9] Chem. Rev. (Ed.: C. L. Hill) 98(Special Issue on Polyoxometalates) (1998) 1–389 .
[10] B. Hasenknopf, Front. Biosci. 10 (2005) 275–287.
[11] D.E. Katsoulis, Chem. Rev. 98 (1998) 359–387.
[12] B. Keita, L. Nadjo, J. Mol. Catal. A 262 (2007) 190–215.
[13] T. Yamase, M.T. Pope (Eds.), Polyoxometalate Chemistry for Nano-Composite Design, Kluwer, Dordrecht, 2002.
[14] D.L. Long, E. Burkholder, L. Cronin, Chem. Soc. Rev. 36 (2007) 105–121.
[15] R.D. Peacock, T.J.R. Weakley, J. Chem. Soc A (1971) 1836–1839.
[16] A. Müller, C. Beugholt, H. Bögge, M. Schmidtmann, Inorg. Chem. 39 (2000) 3112–3113.
[17] L. Cronin, C. Beuggholt, E. Krickemeyer, M. Schmidtmann, H. Bögge, P. Kögerler, T. Kim, K. Luong, A. Müller, Angew. Chem. Int. Ed. 41 (2002) 2805–2808.
[18] C. Howell, F.G. Perez, S. Jain, W.D. Horrocks Jr., A.L. Rheingold, L.C. Francesconi, Angew. Chem. Int. Ed. 40 (2001) 4031–4034.
[19] K. Fukaya, T. Yamase, Angew. Chem. Int. Ed. 42 (2003) 654–658.
[20] D. Drewes, M. Piepenbrink, B. Krebs, Z. Anorg. Allg. Chem. 632 (2006) 534–536.
[21] G.L. Xue, J. Vaissermann, P. Gouzerh, J. Cluster Sci. 13 (2002) 409–421.
[22] P. Mialane, A. Dolbecq, E. Rivière, J. Marrot, F. Sécheresse, Eur. J. Inorg. Chem. (2004) 33–36.
[23] X. Fang, T. Anderson, C. Benelli, C.L. Hill, Chem. Eur. J. 11 (2005) 712–718.
[24] J. Niu, K. Wang, H. Chen, J. Zhao, P. Ma, J. Wang, M. Li, Y. Bai, D. Dang, Cryst. Growth Des. 9 (2009) 4362–4372.
[25] L. Zhongfeng, L. Weisheng, L. Xiaojing, P. Fengkui, L. Yingxia, L. Hao, Magn. Reson. Imaging 25 (2007) 412–417.
[26] (a) F. Hussain, R.W. Gable, M. Speldrich, P. Kögerler, C. Boskovic, Chem. Commun. (2009) 328–330;
(b) F. Hussain, B. Spingler, F. Conrad, M. Speldrich, P. Kögerler, C. Boskovic, G.R. Patzke, Dalton Trans. (2009) 4223–4225;
(c) F. Hussain, F. Conrad, G.R. Patzke, Angew. Chem. 121 (2009) 9252–9255;
(c) F. Hussain, F. Conrad, G.R. Patzke, Angew. Chem. Int. Ed. 48 (2009) 9088–9091;
(d) F. Hussain, G.R. Patzke, CrystEngComm (2010). doi:10.1039/C003489D.
[27] K. Wassermann, M.H. Dickman, M.T. Pope, Angew. Chem. Int. Ed. 36 (1997) 1445–1448.
[28] B.S. Bassil, M.H. Dickman, I. Römer, B. von der Kammer, U. Kortz, Angew. Chem. Int. Ed. Engl. 46 (2007) 6192–6195.
[29] G. Hervé, A. Tézé, Inorg. Chem. 16 (1977) 2115–2117.
[30] CrysAlis Pro software system, Version 171.32; Oxford Diffraction Ltd., Oxford, UK, 2007.
[31] G.M. Sheldrick, Acta. Cryst A64 (2008) 112–122.
[32] U. Kortz, J. Cluster Sci. 14 (2003) 205–214.
[33] R.D. Shannon, Acta Cryst. A32 (1976) 751–767.
[34] (a) T. Moeller, J. Chem. Ed. 47 (1970) 417–424;
(b) D.G. Karraker, J. Chem. Ed. 47 (1970) 424–431.
[35] (a) I.D. Brown, D. Altermatt, Acta Crystallogr. B41 (1985) 244–247;
(b) A. Trzesowska, R. Kruszynski, T.J. Bartczak, Acta Crystallogr. B60 (2004) 174–178.
[36] C. Craciun, L. David, J. Alloys Compd. 323/324 (2001) 743–747.
[37] H. Schilder, H. Lueken, J. Magn. Magn. Mat. 281 (2004) 17–26.
[38] A.J. Shuskus, Phys. Rev. 127 (1962) 2022–2024.
[39] J. Sytsma, K.M. Murdoch, N.M. Edelstein, L.A. Boatner, M.M. Abraham, Phys. Rev. B. 52 (1995) 12668–12676.
[40] (a) E.U. Condon, G.H. Shortley (Eds.), The Theory of Atomic Spectra, Cambridge University Press, Cambridge, 1953;
(b) S. Hüfner (Ed.), Optical Spectra of Transparent Rare Earth Compounds, Academic Press, Inc., New York, 1978.